Paper-Based Sensor for Electrochemical Detection of Silver Nanoparticle Labels by Galvanic Exchange

Josephine C. Cunningham,[†] Molly R. Kogan,[†] Yi-Ju Tsai,[†] Long Luo,[†] Ian Richards,[‡] and Richard M. Crooks*,[†]

[†]Department of Chemistry and the Texas Materials Institute, The University of Texas at Austin, 105 East 24th Street, Stop A5300, Austin, Texas 78712, United States

[‡]Interactives Executive Excellence LLC, 201 North Weston Lane, Austin, Texas 78733, United States

S *Supporting Information*

ABSTRACT: Here we report a three-dimensional paper fluidic device configured for electrochemical detection of biomolecules labeled with silver nanoparticles (AgNPs). This new sensor, which we call a *No*Slip, represents a major improvement of our previously reported *o*Slip system. Specifically, detection of AgNPs in the *No*Slip is based on galvanic exchange rather than a chemical oxidant (bleach or MnO_4^- in the *o*Slip). Galvanic exchange is implemented by depositing a very small amount of gold onto the working electrode. Once the AgNP labels are brought into the proximity of the electrode through the use of magnetic force, a fraction of the Au^0 is electrochemically oxidized to Au^{3+}. The Au^{3+} reacts with the AgNPs to form Ag^+ and Au^0. The Ag^+ is then detected by anodic stripping voltammetry. This new methodology resolves three shortcomings of the *o*Slip while simultaneously simplifying the basic sensor form factor. First, the *No*Slip resolves an oxidant instability issue because of the inherent stability of the Au^0 coating on the electrode that is used to electrogenerate the oxidant (Au^{3+}). Additionally, Au^{3+} is a milder oxidizing agent than bleach or MnO_4^-, so it does not attack the major components of the *No*Slip. Finally, the *No*Slip eliminates the need for a slip layer because the oxidant (Au^{3+}) is electrogenerated on demand. The *No*Slip is able to detect AgNP labels down to concentrations as low as 2.1 pM, the time to result is ~7 min, and the cost at the laboratory scale, not including application-specific reagents, is $0.30.

$$3\ Ag_{(s)} + Au^{3+}_{(aq)} \rightarrow 3Ag^+_{(aq)} + Au_{(s)}$$

KEYWORDS: *electrochemical sensor, silver nanoparticles, anodic stripping voltammetry, paper analytical device, galvanic exchange*
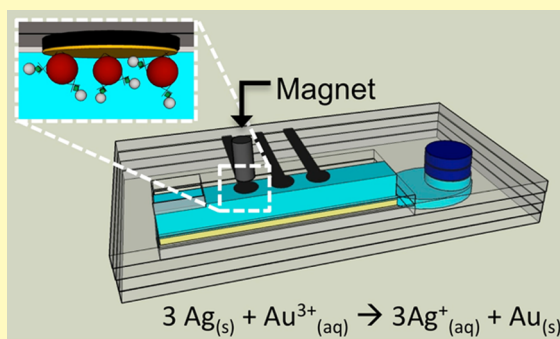
Lateral flow assays (LFAs) were first demonstrated in the 1950s as semiquantitative, colorimetric glucose sensors.[1] Their low cost and simplicity were ideally suited for many applications, and at the present time they dominate the point-of-care (PoC) sensing market.[2,3] LFAs do have limitations that restrict their applications, however. For example, the vast majority provide binary (yes/no) or, at best, semiquantitative output. They are also restricted to simple assays that do not require timed reaction steps, chemical amplification (e.g., polymerase chain reaction), or high degrees of multiplexing. In 2007, Whitesides and co-workers published a seminal paper describing how LFA-like devices could operate in two dimensions.[4] The key insight for that advance was realizing that the tools of photolithography could be used to pattern paper into hydrophilic and hydrophobic domains, thereby directing the flow of aqueous fluids along specified paths in two dimensions and allowing for multiplexed detection.[5−13] The following year the same group showed that this same basic design rule could be expanded to three dimensions,[14] thereby further increasing the number of potential applications.[15−19]

Over the past four years, we have expanded on Whitesides' original multidimensional paper sensing ideas by introducing more convenient fabrication methods based on the principles of origami,[20,21] quantitative detection of analytes at subpicomolar concentrations[22] using on-chip electrochemical methods,[23] hollow channels for faster, more flexible assays,[22−24] and slip layers for timing reactions.[22,25,26] Subsequently, these four developments, in combination with an indirect oxidation strategy,[27−29] came together in a three-dimensional, paper-based sensing device we call an *o*Slip ("o" for origami[20] and "Slip" to indicate that it incorporates a "slip layer").[25,30] The *o*Slip has been used to detect targets, including a model analyte,[22] DNA,[31] and the biological warfare agent ricin.[32] It uses two stages of amplification to achieve detection limits in the low picomolar range at a cost-per-sensor of ~$0.30 at the laboratory scale, not including application-specific reagents.[32] The *o*Slip strategy relies on the target linking together antibody-functionalized magnetic microbeads (MµBs) and silver nanoparticles (AgNPs). The MµBs can be directed

A

toward an electrochemical detection zone by a magnetic force, and the AgNPs can then be detected by indirect oxidation of Ag.

As alluded to above, there are some very desirable aspects of the *o*Slip: low limits of detection (LODs), low cost, scalable fabrication, robust labels (AgNPs, rather than enzymes), time-to-result of <5 min, and relatively simple reconfiguration for different targets. There are, however, three key problems with the *o*Slip. First, a chemical oxidant is required to oxidize the AgNPs, and although we have screened many candidates, none have the necessary stability when dried on paper. Second, the slip layer, which is used for timed delivery of the chemical oxidant, is not user-friendly. Third, although both bleach and permanganate effectively oxidize the AgNP labels, they are very powerful oxidizing agents that also react with other components in real samples and even the *o*Slip itself. We have found this to be problematic for a number of reasons. Accordingly, we sought to develop an alternative design that retains the positive aspects of the *o*Slip while minimizing or eliminating its deficiencies.

The device design that has emerged from our work is called a *No*Slip (Scheme 1) to indicate that the additional slip layer has

Scheme 1

- 🟡 Gold-coated electrode
- ⬤ Carbon electrode
- 🟨 Hemi-channel
- ▢ Unwaxed paper
- ▢ Wax-impregnated paper
- 🔵 Blue dye
- ▢ Paper cut-outs
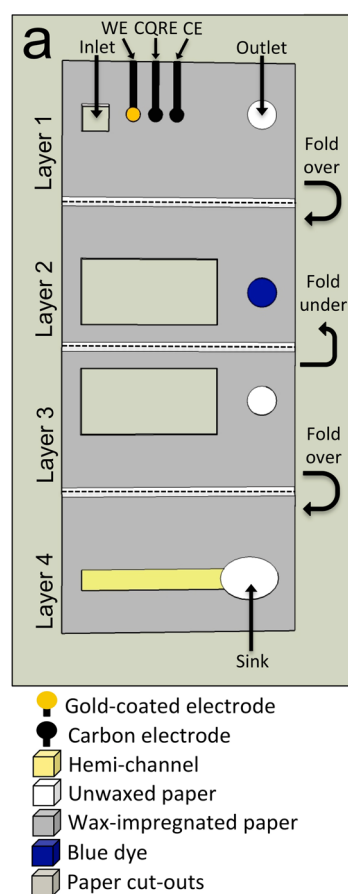
been eliminated. The fabrication and operation of the *No*Slip will be described in detail later, but a few key points are briefly mentioned now. The main shortcomings of the *o*Slip all relate to the presence of a predispensed chemical oxidant, such as permanganate or bleach, so we eliminated the chemical oxidant and now electrogenerate the oxidant on demand. Specifically, Au metal is stored on the device, and it is electrochemically

converted to the oxidant Au^{3+} at the precise time and location needed. This resolves the instability issue, because of the inherent stability of zerovalent Au (Au^0), and it also eliminates the need for the slip layer, because the oxidant is now introduced electrochemically rather than by physical manipulation of a piece of paper. Importantly, the improvements associated with the *No*Slip do not come at the expense of any aspect of device or assay performance.

■ EXPERIMENTAL SECTION

Chemicals and Materials. All solutions were prepared using deionized (DI) water (>18.0 MΩ·cm, Milli-Q Gradient System, Millipore, Bedford, MA). NaCl, NaOH, HCl, HAuCl₄, KNO₃, Na₂SO₄, sodium citrate dihydrate, citric acid monohydrate, urea, 4-(2-hydroxyethyl)-1-piperazineethanesulfonic acid (HEPES), Whatman grade 1 chromatography paper (180 μm thick, 20 cm × 20 cm, linear flow rate (water) of 13 cm/30 min), and siliconized low retention microcentrifuge tubes were all purchased from Fisher Scientific (Pittsburgh, PA). NaHCO₃, K₂HPO₄, and boric acid were purchased from EM Science (Gibbstown, NJ). MgSO₄ and KH₂PO₄ were purchased from EMD Chemicals (Gibbstown, NJ).

A 0.10 M borate solution containing 0.10 M NaCl (referred to hereafter as BCl) was prepared by dissolving the appropriate amount of boric acid and NaCl in DI water, and then adjusting the pH to 7.5 with NaOH. Artificial urine was prepared according to a previously published procedure[33] with a slight modification (1.0 mM of ascorbic acid instead of lactic acid). Citrate-capped AgNPs (nominal 20 nm diameter) and conductive Cu tape (3.0 mm wide) were purchased from Ted Pella (Redding, CA). Erioglaucine disodium salt (blue dye), ascorbic acid, and NH₄Cl were obtained from Acros Organics (Pittsburgh, PA).

Conductive carbon paste (Cl-2042) was purchased from Engineered Conductive Materials (Delaware, OH). Cylindrical neodymium magnets (1/16 in. × 1/2 in., N48) were acquired from Apex Magnets (Petersburg, WV). Streptavidin-coated MμBs (2.8 μm diameter) were obtained from Bangs Laboratories (Fishers, IN). Thiol-DNA-biotin (5′d Thiol C6 SS-ACATTAAAATTC-Biotin 3′) was acquired as a powder from Biosearch Technologies (Petaluma, CA) and, before use, was dissolved in an appropriate volume of DI water to yield a concentration of 1.0 mM. Gold was deposited onto the working electrode of the *No*Slip using a recessed electrochemical cell made of polytetrafluoroethylene (PTFE) equipped with a saturated Hg/Hg₂SO₄ reference electrode (RE), and Pt wire counter electrode (CE) from CH Instruments (Figure S-1).

Instrumentation. All electrochemical measurements were made using a model 700E bipotentiostat from CH Instruments (Austin, TX). A Xerox ColorQube 8570DN printer was used for wax printing. A BioShake iQ (Q Instruments) was used to control mixing during incubation. UV−vis measurements were made with a Hewlett-Packard HP8453 spectrometer and a quartz cell (l = 10.0 mm, 50.0 μL) from Starna Cells (Atascadero, CA).

A Sorvall Legend Micro 21R centrifuge (Thermo Scientific) was used for washing steps during the synthesis of biotinylated AgNPs. A Hitachi S550 scanning electron microscope was used for imaging. The electrode stencil was cut using an Epilog laser engraving system (Zing 16). The 3D-printed holder that encases the *No*Slip (Figure S-2) was designed using Autodesk 123D and printed using polylactic acid (PLA) on a Modified Makerbot Replicator 2s. Adobe Illustrator CS6 (version 16.0.0) was used for the design of the *No*Slip and electrode stencil. The charge under the ASVs was determined by baseline correcting the ASVs using Origin Pro8 SR4 v 8.0951 (Northampton, MA), integrating the area under the peaks, and then dividing by the scan rate.

No*Slip Fabrication. *No*Slips were fabricated as follows. First, a sheet of chromatography paper was patterned with wax (using the wax printer) with multiple *No*Slips (Scheme 1 and Figure S-3a). Second, the sheet of paper was placed (with the wax pattern facing up) into the oven at 130 °C for 30 s to melt the wax through the thickness of the paper to create hydrophobic barriers. Note that the hemichannel on

Scheme 2
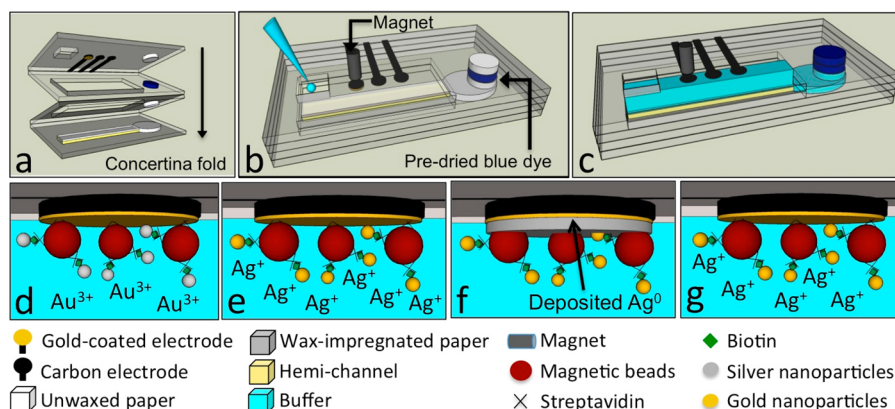
Layer 4 of the *No*Slip (Scheme 1 and Figure S-3a) is made using 60% yellow wax (specified in Adobe Illustrator CS6) that does not melt through the entire thickness of the paper, and therefore creates a hydrophilic floor to drive capillary flow in the *No*Slip hollow channel.[24] Third, the individual devices were cut around the exterior edge and the void spaces on Layers 2 and 3 were removed with a laser cutter. Additional details relating to the fabrication of the electrodes are provided in the Supporting Information.

Preparation of the MμBs-AgNP Composite. Complete details relating to the conjugation of AgNPs to biotin, as well as formation of the AgNP-biotin-streptavidin-MμB composite (referred to hereafter as the "MμB-AgNP composite") are provided in the Supporting Information.

RESULTS AND DISCUSSION

Description of the *No*Slip Design. The *No*Slip platform comprises four wax-printed paper layers, fabricated on a single piece of paper, that are subsequently folded to form the device. As shown in Scheme 1, Layer 1 contains two reservoirs, the inlet and the outlet. The inlet has its cellulose content removed while the outlet retains the unwaxed cellulose paper. In addition, three stencil-printed carbon electrodes are fabricated on the lower face of this layer (face in contact with Layer 2): the working electrode (WE), the carbon quasi-reference electrode (CQRE), and the counter electrode (CE). A small amount of Au is electrodeposited onto the surface of the carbon WE. During device operation, this Au will be oxidized to initiate galvanic exchange with the AgNP labels. Layers 2 and 3 contain *hollow channels* (i.e., the paper is cut out of this region),[24] and Layer 2 also has a paper reservoir loaded with a blue dye. As discussed later, this dye is used to signal cessation of flow through the *hollow channels*. Finally, Layer 4 consists of a hydrophilic layer (*hemichannel*,[34] yellow color) and a sink that drives a continuous flow of fluid through the device until it is saturated with buffer. The *No*Slip is assembled by folding the paper as shown in Schemes 1 and 2a to create a three-dimensional origami paper sensor.

Galvanic Exchange Detection Method. In galvanic exchange reactions, a zerovalent first metal reacts with the ions of a second, more noble metal. If the redox potentials of the metals are sufficiently different, this results in oxidation of the first metal and reduction of the second. In the present case, the first metal is AgNPs and the second metal ions are Au^{3+}. The relevant redox reaction is given by eq 1.

$$3Ag_{(s)} + Au^{3+}_{(aq)} \rightarrow 3Ag^{+}_{(aq)} + Au_{(s)} \tag{1}$$
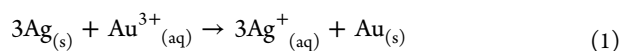
Under standard conditions, the driving force for eq 1 is just the difference in the standard potentials of the individual half reactions: $\Delta E = 0.70$ V.[35] This is sufficient overpotential to drive eq 1 to completion.

We are interested in developing assays for specific targets that rely on detection of AgNP labels via a galvanic exchange mechanism. As a preliminary step in that direction, we carried out a proof-of-concept assay using the *No*Slip and a model analyte consisting of AgNPs linked to MμBs via biotin–streptavidin conjugation: the MμB-AgNP composite. In the future, the conjugate will be an antibody or DNA sandwich, or any other specific binding reaction of interest. The general operation of the *No*Slip is shown in Scheme 2. Once the device is assembled, the sample (50 μL) is loaded at the inlet (Scheme 2b). Capillary flow, driven by the hydrophilic *hemichannel*, commences immediately, driving the sample down the open channel toward the sink (Scheme 2c). As the sample passes the working electrode, the magnet localizes the MμB-AgNP composite under the working electrode. When the sink becomes full, upward flow is initiated through the paper reservoir at the end of Layer 3 and toward the outlet. This rehydrates the dye on Layer 2 and a blue color appears at the outlet, indicating that flow has stopped (Scheme 2c) and that galvanic exchange detection can be initiated.

Scheme 2d–g illustrates how the galvanic exchange process plays out. Scheme 2d shows the MμB-AgNP composite trapped at the working electrode. The first step in the detection process is the application of a 50.0 s potential step (from the open circuit potential (OCP) to 0.30 V vs CQRE) to the Au-modified working electrode. This results in conversion of Au^0 to Au^{3+}. A key feature of the *No*Slip is that this oxidant is formed exactly where it is required: adjacent to the trapped AgNPs. Moreover, the oxidizing power of Au^{3+} is sufficient to oxidize Ag, but, as far as we know, it is not so strong as to interact with other components of the *No*Slip or the buffer present in the channel. Scheme 2e shows that eq 1 now proceeds spontaneously to yield Ag^+. A second potential step from 0.30 V to −0.70 V for 200.0 s results in electrodeposition of metallic Ag onto the working electrode (Scheme 2f). Residual (i.e., unreacted) Au^{3+} is also electrodeposited as Au^0 at this potential. In the last detection step (Scheme 2g), bulk, Ag^0 is electrochemically oxidized at the working electrode surface by scanning the WE potential from −0.70 to 0.20 V vs CQRE. Integration of the area under the peak in the resulting current transient corresponds to the charge contained in the AgNP labels, and hence it reflects the original concentration of the
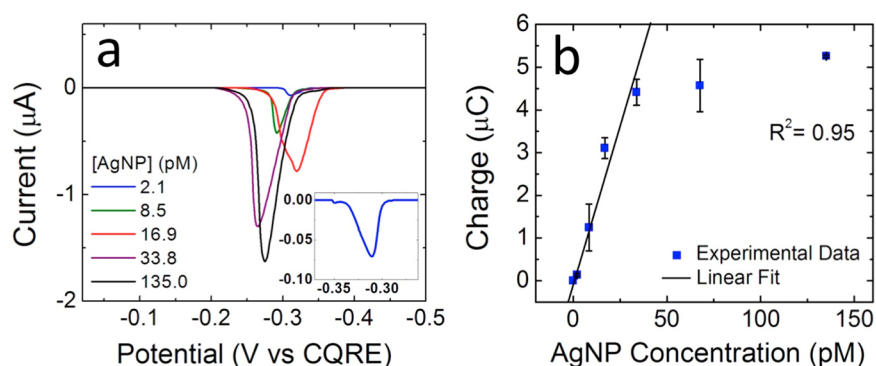
Figure 1. Electrochemical ASV results for detection of the MμB-AgNP composite in 0.10 M BCl solution using the *No*Slip. (a) Second ASVs recorded for the concentrations of AgNP labels shown in the legend. The inset shows an expanded view of the ASV obtained for 2.1 pM AgNPs. The scan rate was 0.010 V/s, and scans started at −0.70 V and ended at 0.20 V. The ASVs were corrected for a sloping baseline that results from oxygen reduction. (b) Calibration curve showing the correlation between charge (obtained by integrating ASVs like those in (a)) and the concentration of AgNPs. Each data point represents the average of at least three measurements carried out using independently fabricated *No*Slips. The error bars represent the standard deviation of those measurements. The black line is the best linear fit to the data points, weighted by the error bars.
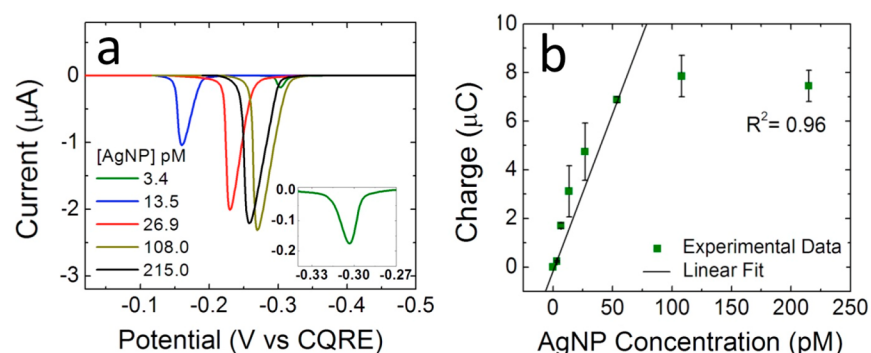
Figure 2. Electrochemical ASV results for detection of the MμB-AgNP composite in artificial urine using the *No*Slip. (a) Second ASVs for the concentrations of AgNP labels shown in the legend. The inset shows an expanded view of the ASV obtained for 3.4 pM AgNPs. The scan rate was 0.010 V/s, and scans started at −0.70 V and ended at 0.20 V. The ASVs were corrected for a sloping baseline that results from oxygen reduction. (b) Calibration curve showing the correlation between charge (obtained by integrating ASVs like those in (a)) and the concentration of AgNPs. Each data point represents the average of at least three measurements carried out using independently fabricated *No*Slips. The error bars represent the standard deviation of those measurements. The black line is the best linear fit to the data points, weighted by the error bars.

analyte. One final point: In the absence of galvanic exchange, no Ag signal is observed even at high AgNP concentrations. In other words, there is no direct oxidation of AgNPs at the working electrode, and therefore this galvanic exchange approach is a zero-background detection method.

The *No*Slip detection approach retains the double-amplification methodology we previously introduced in the *o*Slip.[22,31,32] The first amplification step corresponds to preconcentration of the AgNP labels at the electrode surface using magnetic force. The second corresponds to the 250 000 equiv of charge present in each 20-nm-diameter AgNP. Importantly, however, the use of galvanic exchange, in place of chemical oxidation by (for example) KMnO₄, greatly increases the robustness of the assay. This is because Au is stored in its highly stable metallic form until it is required to oxidize the AgNPs. Even more important, this approach removes the need for the slip layer, thereby eliminating a user-initiated step in the assay. In short, the *No*Slip represents another significant advance in the field of paper fluidics.

Galvanic Exchange Detection Performance on the *No*Slip. Using the process described in the previous section, we collected anodic stripping voltammograms (ASVs) after injecting different concentrations of the MμB-AgNP composite into *No*Slip sensors (Figure 1a). For reasons we will discuss

later, we collected two ASVs for each concentration and used the second one for the analysis. The *No*Slips are disposable, so each experiment was carried out using a different device. The observed shifts in ASV peak potentials are likely due to the CQRE, which is not as stable as a real reference electrode. This is not a big problem for the *No*Slip, however, because there are no other species oxidized within the potential range of the ASV peak positions.

The dose–response curve in Figure 1b shows the relationship between charge (measured under ASV peaks like those in Figure 1a) and AgNP concentration. Between 2.1 and 33.8 pM the plot is linear, but at higher AgNP concentrations the dose–response curve plateaus, suggesting that insufficient Au³⁺ was created to fully oxidize the AgNPs during galvanic exchange. The important point, however, is that even at this very early stage of development, the pre-prototype *No*Slip is able to detect 2.1 pM of the AgNP labels with a device-to-device coefficient of variation (CV) of 15.8% (average of the standard deviation divided by the mean for all AgNP concentrations in the MμB-AgNP composite), a sample-to-result time of ~7 min, and a collection efficiency of 16.8% (charge collected divided by charge-equivalents injected into the *No*Slip).

As mentioned earlier, one of the problems we experienced with the *o*Slip was that the strong chemical oxidant (e.g., bleach

or permanganate) oxidized components of the target matrix in addition to the AgNPs. In contrast, Au^{3+} is a milder oxidizing agent, so we reasoned that this problem would be minimized in the *No*Slip. To test this hypothesis, we carried out *No*Slip experiments using artificial urine as the matrix rather than BCl solution. The composition of artificial urine is described in the Experimental Section, but briefly, the four principal components are urea (170 mM), NaCl (90 mM), $NaHCO_3$ (25 mM), and NH_4Cl (25 mM). None of these are electroactive in the potential range used in the galvanic exchange/ASV analysis, so they do not interfere with the assay. However, ascorbic acid is present at a low concentration of 1.0 mM and, as shown in Figure S-4, its oxidation onset potential is close to that of Au^0. This could be problematic, because co-oxidation of ascorbic acid and Au^0 results in less than 100% current efficiency for Au^0 oxidation. By careful selection of the potential used for Au^0 oxidation (0.30 V vs CQRE) this possible problem is largely avoided.

For the artificial urine experiments, the same procedure used for the buffer experiments was followed, except the MμB-AgNP composite was resuspended in 50.0 μL of artificial urine after the third washing step. Figure 2a shows the resulting ASVs for a range of AgNP label concentrations. As discussed earlier, the location of the ASV peak is not constant due to the instability of the quasi-reference electrode, but this has no practical effect on the assay. Figure 2b is a dose−response curve that was generated by integrating ASVs like those in Figure 2a. The linear range in artificial urine is from 3.4 to 53.8 pM AgNPs, which is comparable to that found in buffer: 2.1 to 33.8 pM AgNPs (Figure 1b). The lowest detectable concentrations of AgNPs in artificial urine and buffer are also comparable: 3.4 pM and 2.1 pM, respectively. Note that because the *No*Slip is a zero-background method it is not possible to calculate a well-defined limit of detection.

A Closer Look at Galvanic Exchange. The galvanic exchange process is somewhat more complicated than we have thus far alluded to. This additional complexity does not affect the *No*Slip assay to any great degree, but it is interesting and relevant and therefore requires some further explanation.

During the electrochemical detection procedure, an excess number of equivalents of Au^{3+} (relative to Ag^0) are electro-generated to ensure that the galvanic exchange process goes to completion. This means that after the AgNPs, which are localized near the electrode surface, are fully oxidized to Ag^+, Au^{3+} is also present in the vicinity of the working electrode. Accordingly, when the electrode potential is stepped negative to reduce Ag^+, Au^0 is codeposited resulting in the likely formation of a AgAu alloy. Moreover, due to the inhomogeneous distribution of Au^{3+} and Ag^+ in the diffusion layer, and because of the large excess of Au^{3+}, Au^0 preferentially deposits on the electrode toward the end of the electrodeposition period. This results in formation of a (primarily) Au^0 shell capping the electrodeposited AgAu alloy. As shown in Scheme 3a, this renders the underlying Ag^0 electrochemically inaccessible. Note that the innermost core of Au^0 shown in Scheme 3a was deposited during initial device fabrication (see Experimental Section and also Figure S-5).

The presence of this structure means that during the first ASV scan following codeposition of Ag^0 and Au^0, the Ag ASV peak is either small or nonexistent as illustrated by the black voltammogram in Figure 3. However, after obtaining the first ASV, the working electrode potential is stepped back to −0.70 V, and a second ASV scan is initiated using the same

Scheme 3
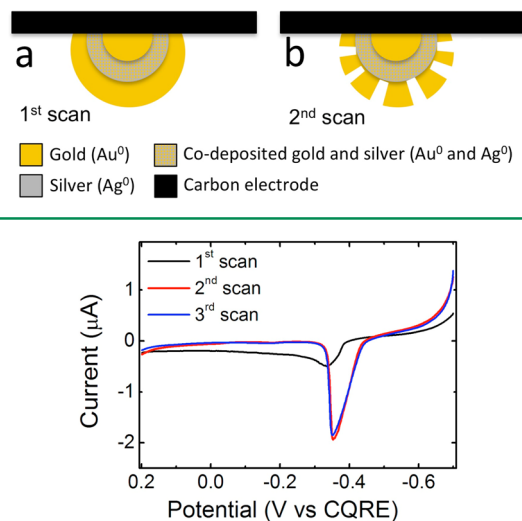
Figure 3. Three consecutive ASVs following the coelectrodeposition of Au^0 and Ag^0. The first ASV was obtained by scanning the electrode potential from −0.70 to 0.20 V at a scan rate of 0.010 V/s in 0.10 M BCl solution. The second and third ASVs were obtained by immediately stepping the electrode potential back to −0.70 V at the end of the previous scan, and promptly starting the next scan.

parameters as for the first. The result is the red trace in Figure 3, which exhibits a much larger current than the first ASV. The second peak is larger than the first because during the last part of the first scan (between −0.20 and 0.20 V) a little of the Au^0 overlayer is oxidized (see Figure S-6) allowing the underlying Ag^0 to be accessed electrochemically. This situation is illustrated in Scheme 3b.

The really interesting finding is that if a third ASV is obtained (blue trace, Figure 3) using the same procedure as for the first and second, another Ag ASV peak is observed, and it has nearly the same shape and height as the second. This result is surprising, because one would anticipate that after each scan some Ag^+ would be lost due to diffusion away from the working electrode and the corresponding incomplete redeposition of Ag^0. We hypothesized that this strange result is a consequence of the presence of 0.10 M Cl^- in the electrolyte solution, and hence precipitation of $AgCl_{(s)}$ ($K_{sp} = 1.8 \times 10^{-10}$)[36] onto the electrode surface.

Clearly, it is crucial to understand the underlying mechanism of the galvanic exchange procedure, because it is at the heart of the *No*Slip methodology. Accordingly, we undertook a number of experiments to confirm or refute the $AgCl_{(s)}$ precipitation hypothesis. In the first of these, a series of experiments was carried out in which the electrodeposition time was varied between 50.0 and 200.0 s, and then the first and second ASVs were recorded. The methodology for these experiments was very similar to those used to obtain the data in Figure 1: a separate *No*Slip device for each experiment and injection of 50.0 μL of 33.8 pM MμB-AgNP composite present in 0.10 M BCl solution.

Figure 4 shows the results of this experiment, and our interpretation is illustrated on the left side of the figure. The charge under the ASV peak of the first scan increases up to electrodeposition times of 100.0 s, and then it decreases. As shown on the left side of Figure 4, we believe that codeposition of Ag^0 and Au^0 occurs at shorter times, but at longer times the
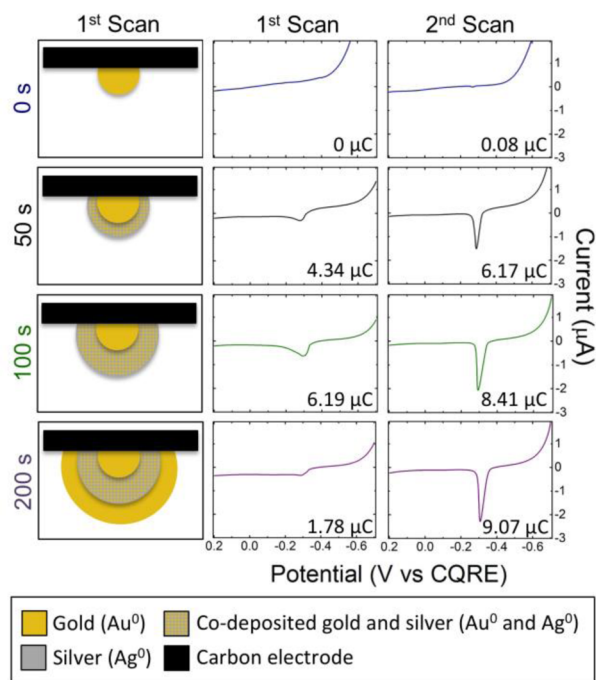
Figure 4. Effect of electrodeposition time on the ASV peak size and shape for the first and second scans. Following galvanic exchange, the potential was held at −0.70 V for the times indicated on the left side of the figure, scanned from −0.70 to 0.20 V at a scan rate of 0.010 V/s to obtain the first ASVs, and then the potential was immediately rescanned from −0.70 to 0.20 V at 0.010 V/s to obtain the second ASVs. All ASVs were collected using 33.8 pM of AgNP labels in the MμB-AgNP composite suspended in 0.10 M BCl solution.

Ag^+ is largely depleted and primarily only Au^{3+} is electrodeposited. This results in deposition of a protective shell of mostly Au^0 (bottom frame of Figure 4) that limits the amount of Ag^0 that can be oxidized during the first ASV. As discussed earlier, however, some of the Au^0 shell is oxidized at the end of the first ASV scan (between −0.20 and 0.20 V), and this leaves some Ag^0 exposed that can be oxidized during the second scan. Therefore, there is a consistent increase in the charge due to Ag^0 oxidation as a function of the electrodeposition time during the second scan (right side of Figure 4).

Notice also that, at all times (50.0−200.0 s), the Ag ASV peaks are noticeably sharper for the second scans compared to the first. The broad peaks in the first scans indicate that Ag is more difficult to oxidize, which may be due to Ag^0 being in the form of an AgAu alloy. We hypothesize that immediately following galvanic exchange, some of the Ag^+ will precipitate as $AgCl_{(s)}$, but a large portion of the Cl^- is already consumed by the excess gold as $AuCl_4^-$; therefore, the majority of the Ag^0 will deposit onto the electrode as a AgAu alloy. Following codeposition of Ag^0 and Au^0 on the WE, the bulk concentration of free Cl^- is re-established in the vicinity of the electrode. Accordingly, a large percentage of the Ag^+ that is oxidized during the first ASV scan likely forms $AgCl_{(s)}$. The second-scan Ag ASV peaks are sharper due to the fast kinetics of the Ag^0 to AgCl redox reaction.[35]

Recall that we invoked the importance of aqueous Cl^- in our interpretation of the ASVs in Figures 3 and 4, and we claimed that the limited solubility of AgCl is responsible for the observation that ASVs subsequent to the first scan are nearly identical. To test this hypothesis, a 50.0 μL aliquot of 0.75 nM citrate-stabilized (no Cl^- present) AgNPs (i.e., not conjugated

to thiol-DNA-biotin) were injected into a *No*Slip and the galvanic exchange electrochemical procedure was followed as described in the Experimental Section with a single modification: the first 50.0 s potential step was from OCP to 0.60 V vs CQRE rather than to 0.30 V. This modification was necessary because in the absence of Cl^- a more positive potential is required to oxidize Au^0.

The first and second ASVs resulting from this experiment are displayed in Figure 5. Clearly, both ASV peaks are small, which
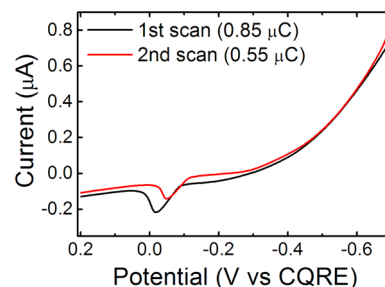
Figure 5. Consecutive ASVs in the absence of MμBs and Cl^-. The ASVs were collected by injecting 50 μL of a 0.75 nM solution of citrate-stabilized AgNPs into a *No*Slip. The black trace is the first ASV and the red trace is the second ASV. The scan rate was 0.010 V/s and the electrolyte was 2.0 mM citrate buffer (pH 7.4). The potential was initially held at 0.60 V for 50.0 s, then held at −0.70 V for 200.0 s, and then scanned from −0.70 to 0.20 V two successive times at a scan rate of 0.010 V/s.

is a consequence of the absence of the MμBs and hence absence of AgNP localization near the WE. The more important point, however, is that the second Ag ASV peak is significantly smaller than the first. This is because $AgCl_{(s)}$ cannot form in the absence of Cl^-, and therefore Ag^+ is able to diffuse away from the electrode rather than precipitate in its proximity. The data in Figure 5 confirm the original hypothesis and clearly illustrate the importance of Cl^- for this assay. Additional information that supports the mechanism of the galvanic exchange detection strategy is provided in the Supporting Information.

■ SUMMARY AND CONCLUSION

Our original origami paper sensor, the *o*Slip, suffered from three problems: (1) it was necessary to use chemical oxidants (e.g., bleach or permanganate), which have poor stability when dried on paper; (2) bleach and permanganate are very strong oxidizing agents that react with other components in the system, including the *o*Slip itself; and (3) the slip layer, which is needed for timed delivery of the chemical oxidant, was not user-friendly. By changing the means by which the AgNP labels are oxidized (galvanic exchange vs chemical oxidation with a reagent like MnO_4^-), all three of these issues have been resolved with only minor (simplifying) changes to the basic form factor of the platform and no significant change in performance. Specifically, the *No*Slip resolves the oxidant instability issues because of the inherent stability of the Au^0 coating on the electrode that is used to electrogenerate the oxidant (Au^{3+}). Additionally, Au^{3+} is a milder oxidizing agent than bleach or permanganate, so it does not noticeably react with other components of the *No*Slip. Finally, the *No*Slip eliminates the need for the slip layer because the oxidant (Au^{3+}) is electrogenerated on demand.

The *No*Slip is inexpensive (not including application-specific reagents, the laboratory-scale cost is ~$0.30 per device), the on-chip assay time is ~7 min, it requires no user intervention other than sample placement, and it is able to detect label concentrations as low as 2.1 pM. Importantly, the *No*Slip sensor can be configured to detect a variety of target molecules, including proteins,[32] DNA,[31] bacteria, and viruses, if appropriate capture agents are available. Looking to the future, we plan to devise specific assays that take advantage of the sensitivity and design flexibility of the *No*Slip, we are working with collaborators to develop a dedicated reader that eliminates the need for a research-grade potentiostat, and we are developing methods for incorporating assay reagents directly onto the *No*Slip to eliminate the need for off-chip sample manipulation. The results of these experiments will be reported in due course.

ASSOCIATED CONTENT

Ⓢ Supporting Information

The Supporting Information is available free of charge on the ACS Publications website at DOI: 10.1021/acssensors.5b00051.

> RevSI-Model NoSlip-092315. Electrochemical cell for gold electrodeposition on the *No*Slip working electrode; 3D printed holder design and dimensions; *No*Slip and electrode stencil dimensions; *No*Slip electrode fabrication; co-oxidation of Au and ascorbic acid; scanning electron micrographs of working electrode; oxidation of Au overlayer to expose Ag; protocol for AgNP-biotin conjugation; protocol for binding AgNP-biotin to MµB-streptavidin; ASVs in smaller potential windows prevent Au reoxidation; redeposition of Ag in between ASVs; and effect of scan rate on Ag ASVs (PDF)

AUTHOR INFORMATION

Corresponding Author

*E-mail: crooks@cm.utexas.edu. Tel: 512-475-8674.

Notes

The authors declare no competing financial interest.

ACKNOWLEDGMENTS

ABBREVIATIONS

AgNP, silver nanoparticle; LFAs, lateral flow assays; PoC, point-of-care; MµBs, magnetic microbeads; LODs, limits of detection; BCl, borate and chloride solution; PTFE, polytetrafluoroethylene; RE, reference electrode; CE, counter electrode; WE, working electrode; PLA, polylactic acid; CQRE, carbon quasi-reference electrode; OCP, open circuit potential; ASVs, anodic stripping voltammograms; CV, coefficient of variation

REFERENCES

(1) Free, A. H.; Adams, E. C.; Kercher, M. L.; Free, H. M.; Cook, M. H. Simple specific test for urine glucose. *Clin. Chem.* **1957**, *3*, 163−168.

(2) Posthuma-Trumpie, G.; Korf, J.; van Amerongen, A. Lateral Flow (immuno)assay: Its Strengths, Weaknesses, Opportunities and Threats. A Literature Survey. *Anal. Bioanal. Chem.* **2009**, *393*, 569−582.

(3) Gubala, V.; Harris, L. F.; Ricco, A. J.; Tan, M. X.; Williams, D. E. Point of Care Diagnostics: Status and Future. *Anal. Chem.* **2012**, *84*, 487−515.

(4) Martinez, A. W.; Phillips, S. T.; Butte, M. J.; Whitesides, G. M. Patterned Paper as a Platform for Inexpensive, Low-Volume, Portable Bioassays. *Angew. Chem., Int. Ed.* **2007**, *46*, 1318−1320.

(5) Wu, Y.; Xue, P.; Kang, Y.; Hui, K. M. Paper-Based Microfluidic Electrochemical Immunodevice Integrated with Nanobioprobes onto Graphene Film for Ultrasensitive Multiplexed Detection of Cancer Biomarkers. *Anal. Chem.* **2013**, *85*, 8661−8668.

(6) Wu, Y.; Xue, P.; Hui, K. M.; Kang, Y. A Paper-Based Microfluidic Electrochemical Immunodevice Integrated with Amplification-by-Polymerization for the Ultrasensitive Multiplexed Detection of Cancer Biomarkers. *Biosens. Bioelectron.* **2014**, *52*, 180−187.

(7) Hossain, S. M. Z.; Brennan, J. D. B-Galactosidase-Based Colorimetric Paper Sensor for Determination of Heavy Metals. *Anal. Chem.* **2011**, *83*, 8772−8778.

(8) Mentele, M. M.; Cunningham, J.; Koehler, K.; Volckens, J.; Henry, C. S. Microfluidic Paper-Based Analytical Device for Particulate Metals. *Anal. Chem.* **2012**, *84*, 4474−4480.

(9) Dungchai, W.; Chailapakul, O.; Henry, C. S. Use of Multiple Colorimetric Indicators for Paper-Based Microfluidic Devices. *Anal. Chim. Acta* **2010**, *674*, 227−233.

(10) Evans, E.; Moreira Gabriel, E. F.; Benavidez, T. E.; Tomazelli Coltro, W. K.; Garcia, C. D. Modification of Microfluidic Paper-Based Devices with Silica Nanoparticles. *Analyst* **2014**, *139*, 5560−5567.

(11) Cate, D. M.; Noblitt, S. D.; Volckens, J.; Henry, C. S. Multiplexed Paper Analytical Device for Quantification of Metals Using Distance-Based Detection. *Lab Chip* **2015**, *15*, 2808−2818.

(12) Vella, S. J.; Beattie, P.; Cademartiri, R.; Laromaine, A.; Martinez, A. W.; Phillips, S. T.; Mirica, K. A.; Whitesides, G. M. Measuring Markers of Liver Function Using a Micropatterned Paper Device Designed for Blood from a Fingerstick. *Anal. Chem.* **2012**, *84*, 2883−2891.

(13) Lafleur, L.; Stevens, D.; McKenzie, K.; Ramachandran, S.; Spicar-Mihalic, P.; Singhal, M.; Arjyal, A.; Osborn, J.; Kauffman, P.; Yager, P.; et al. Progress toward Multiplexed Sample-to-Result Detection in Low Resource Settings Using Microfluidic Immunoassay Cards. *Lab Chip* **2012**, *12*, 1119−1127.

(14) Martinez, A. W.; Phillips, S. T.; Whitesides, G. M. Three-Dimensional Microfluidic Devices Fabricated in Layered Paper and Tape. *Proc. Natl. Acad. Sci. U. S. A.* **2008**, *105* (50), 19606−19611.

(15) Rattanarat, P.; Dungchai, W.; Cate, D.; Volckens, J.; Chailapakul, O.; Henry, C. S. Multilayer Paper-Based Device for Colorimetric and Electrochemical Quantification of Metals. *Anal. Chem.* **2014**, *86*, 3555−3562.

(16) Schonhorn, J. E.; Fernandes, S. C.; Rajaratnam, A.; Deraney, R. N.; Rolland, J. P.; Mace, C. R. A Device Architecture for Three-Dimensional, Patterned Paper Immunoassays. *Lab Chip* **2014**, *14*, 4653−4658.

(17) Ge, S.; Liu, W.; Ge, L.; Yan, M.; Yan, J.; Huang, J.; Yu, J. In Situ Assembly of Porous Au-Paper Electrode and Functionalization of Magnetic Silica Nanoparticles with HRP via Click Chemistry for Microcystin-LR Immunoassay. *Biosens. Bioelectron.* **2013**, *49*, 111−117.

(18) Wang, H.; Li, Y.; Wei, J.; Xu, J.; Wang, Y.; Zheng, G. Paper-Based Three-Dimensional Microfluidic Device for Monitoring of Heavy Metals with a Camera Cell Phone. *Anal. Bioanal. Chem.* **2014**, *406*, 2799−2807.

(19) Cate, D. M.; Adkins, J. A.; Mettakoonpitak, J.; Henry, C. S. Recent Developments in Paper-Based Microfluidic Devices. *Anal. Chem.* **2015**, *87*, 19−41.

(20) Liu, H.; Crooks, R. M. Three-Dimensional Paper Microfluidic Devices Assembled Using the Principles of Origami. *J. Am. Chem. Soc.* **2011**, *133*, 17564−17566.

(21) Liu, H.; Xiang, Y.; Lu, Y.; Crooks, R. M. Aptamer-Based Origami Paper Analytical Device for Electrochemical Detection of Adenosine. *Angew. Chem., Int. Ed.* **2012**, *51*, 6925−6928.

(22) Scida, K.; Cunningham, J. C.; Renault, C.; Richards, I.; Crooks, R. M. Simple, Sensitive, and Quantitative Electrochemical Detection Method for Paper Analytical Devices. *Anal. Chem.* **2014**, *86*, 6501−6507.

(23) Renault, C.; Anderson, M. J.; Crooks, R. M. Electrochemistry in Hollow-Channel Paper Analytical Devices. *J. Am. Chem. Soc.* **2014**, *136*, 4616−4623.

(24) Renault, C.; Li, X.; Fosdick, S. E.; Crooks, R. M. Hollow-Channel Paper Analytical Devices. *Anal. Chem.* **2013**, *85*, 7976−7979.

(25) Liu, H.; Li, X.; Crooks, R. M. Paper-Based SlipPAD for High-Throughput Chemical Sensing. *Anal. Chem.* **2013**, *85*, 4263−4267.

(26) Cunningham, J. C.; Brenes, N. J.; Crooks, R. M. Paper Electrochemical Device for Detection of DNA and Thrombin by Target-Induced Conformational Switching. *Anal. Chem.* **2014**, *86*, 6166−6170.

(27) Szymanski, M. S.; Porter, R. A. Preparation and Quality Control of Silver Nanoparticle−antibody Conjugate for Use in Electrochemical Immunoassays. *J. Immunol. Methods* **2013**, *387*, 262−269.

(28) Authier, L.; Grossiord, C.; Brossier, P.; Limoges, B. Gold Nanoparticle-Based Quantitative Electrochemical Detection of Amplified Human Cytomegalovirus DNA Using Disposable Microband Electrodes. *Anal. Chem.* **2001**, *73*, 4450−4456.

(29) Szymanski, M.; Turner, A. P. F.; Porter, R. Electrochemical Dissolution of Silver Nanoparticles and Its Application in Metalloimmunoassay. *Electroanalysis* **2010**, *22*, 191−198.

(30) Du, W.; Li, L.; Nichols, K. P.; Ismagilov, R. F. SlipChip. *Lab Chip* **2009**, *9*, 2286−2292.

(31) Li, X.; Scida, K.; Crooks, R. M. Detection of Hepatitis B Virus DNA with a Paper Electrochemical Sensor. *Anal. Chem.* **2015**, *87* (17), 9009−9015.

(32) Cunningham, J. C.; Scida, K.; Kogan, M. R.; Wang, B.; Ellington, A. D.; Crooks, R. M. Paper Diagnositc Device for Quantitative Electrochemical Detection of Ricin at Picomolar Levels. *Lab Chip* **2015**, *15*, 3707−3715.

(33) Brooks, T.; Keevil, C. W. A Simple Artificial Urine for the Growth of Urinary Pathogens. *Lett. Appl. Microbiol.* **1997**, *24*, 203−206.

(34) Renault, C.; Koehne, J.; Ricco, A. J.; Crooks, R. M. Three-Dimensional Wax Patterning of Paper Fluidic Devices. *Langmuir* **2014**, *30*, 7030−7036.

(35) Bard, A. J.; Faulkner, L. R. *Electrochemical Methods*, 2nd ed.; Wiley: New York, 2001.

(36) Harris, D. C. *Quantitative Chemical Analysis*, 8th ed.; W. H. Freeman, 2011.